Arias Intensity Attenuation Relationship in Sichuan-yunnan Region, China

Ping Liu (liuping1005@xust.edu.cn)
School of Architecture and Civil Engineering, Xi'an University of Science and Techology
https://orcid.org/0000-0001-6786-4696

Tongjie Ren
Xi'an University of Science and Technology https://orcid.org/0000-0001-9357-190X

Research Article

Keywords: Arias intensity, earthquake-induced landslide, Sichuan-Yunnan region, attenuation relationship

Posted Date: December 2nd, 2021

DOI: https://doi.org/10.21203/rs.3.rs-1129750/v1

Arias intensity attenuation relationship in Sichuan-Yunnan region, China

Ping Liu[1], and Tongjie Ren[1]

Abstract Arias intensity is an essential ground motion measure correlating with the potential for earthquake-induced landslides. The Sichuan-Yunnan region, which is primarily mountainous, is a high incidence region of earthquake-induced landslides in China. However, there is no available attenuation relationship for this intensity measure due to the backward construction of the stations. In this study, we developed a region-specific Arias intensity attenuation relationship using the China Strong-Motion Networks Center (CSMNC) database which was established in 2008. We recommend this relationship be applied in the Sichuan-Yunnan region for moment magnitudes ranging between 4.2 and 7.9, distances ranging between 0 and 400 km and with V_{s30} (the average shear-wave velocity in the upper 30 meters of a soil profile) ranging between 128 and 760 m/s. The current study finds that this relationship's intra-event, inter-event, and total standard deviations are greater than for other regions. This is likely caused by the complicated seismotectonic activities, nonlinear site effects, error from inferring V_{s30}, basin effects, etc. However, this relationship has the best performance in fitting and predicting the data from the Sichuan-Yunnan region.

Keywords Arias intensity; earthquake-induced landslide; Sichuan-Yunnan region; attenuation relationship

✉ Ping Liu
liuping1005@xust.edu.cn
✉ Tongjie Ren
angelren0@163.com

1 School of Architecture and Civil Engineering, Xi'an University of Science and Technology, Xi'an 710054, China

1. Introduction

Arias intensity (Arias, 1970) contains amplitude, duration, and frequency and is an essential ground motion measure for correlating earthquake damage potential, especially the Newmark displacement of earthquake-induced landslides (Jibson 1993; Jibson and 1998; Romeo 2000; Jibson 2007; Rathje and Saygili 2008; Hsieh and Lee 2011; Jin et al. 2018), lends itself to application in probabilistic seismic hazard analysis (PSHA) of earthquake-induced landslides (Chousianitis et al. 2014; Wang et al. 2016; Wang et al. 2017; Yue et al. 2018; Lu et al. 2019). The attenuation relationship (or predictive equation), which considers various factors (e.g. source, path, site, etc.), is one of the main approaches for estimating the Arias intensity. Many researchers have proposed the Arias intensity attenuation relationship in other regions (e.g. Travasarou et al. 2003; Hwang et al. 2004; Stafford et al. 2009; Rajabi et al. 2010; Campbell and Bozorgnia 2012; Foulser-Piggott and Stafford 2012; Lee et al. 2012; Chousianitis et al. 2014; Foulser-Piggott and Goda 2015; Liu et al. 2015; Liu et al. 2016; Sandıkkaya and Akkar 2016; Campbell and Bozorgnia 2019; Bahrampouri et al. 2020).

The Sichuan-Yunnan region located in the southwest of China is one of China's most seismically active regions. During the Cenozoic, the Sichuan basin was hindering the Indian plate from squeezing the Eurasian plate, resulting in many fault zones such as the Longmenshan Thrusts zone (Fig. 1). The east boundary of the Sichuan-Yunnan faulted-block (Tapponnier et al. 1982; Zhang et al. 2003) formed a substantial left-lateral strike-slip fault system with a total length of more than 1100 km named the "Kangding fault" system (Tapponnier and Molnar 1977). Allen et al. (1991) and Wen et al. (2000) investigated the history of earthquakes in the Sichuan-Yunnan region that had occurred over a period of hundreds of years and the active strike-slip fault zones in the intra-plate area of China and found that intensive seismotectonic activities often appear around the "Kangding fault" system.

The Sichuan-Yunnan region, primarily mountainous, is a high incidence region of earthquake-induced landslides leading to massive casualties and economic losses (e.g. 197,481 landslides in the 2008 Wenchuan M_w 7.9 earthquake (Xu and Xu 2013); 22,528 landslides in the 2013 Lushan M_w 6.8 earthquake (Xu et al. 2015); 10,559 landslides in the 2016 Ludian M_w 6.2 earthquake (Wu and Xu 2018); 4800 landslides in the 2017 Jiuzhaigou M_w 6.5 earthquake (Xu et al. 2018)). Due to the backward construction of the station, there was a lack of strong-motion recordings in this region before 2000. The China Strong-Motion Networks Center (CSMNC) system completed in March 2008 has collected a significant amount of high-quality digital strong-motion recordings in this region, including numerous near-field recordings of large earthquakes such as the Wenchuan M_w 7.9 earthquake. The collection of these useful recordings is benefiting from a dense strong motion station distribution. Those recordings have greatly enriched the strong-motion database in China and enabled the establishment of the Arias intensity attenuation relationship in the Sichuan-Yunnan region.

In this study, we developed a region-specific Arias intensity attenuation relationship in the Sichuan-Yunnan region, considering source effects (magnitude and focal mechanism), path effects (source to site distance), and site effects (V_{s30}, the average shear-wave velocity in the upper 30 meters of a soil profile). Through model comparison, uncertainty analysis, and model testing we explored the accuracies of estimation and prediction of this model. This study is of great significance to the seismic risk analysis of earthquake-induced landslides in Southwest China, which is the intention of our work.

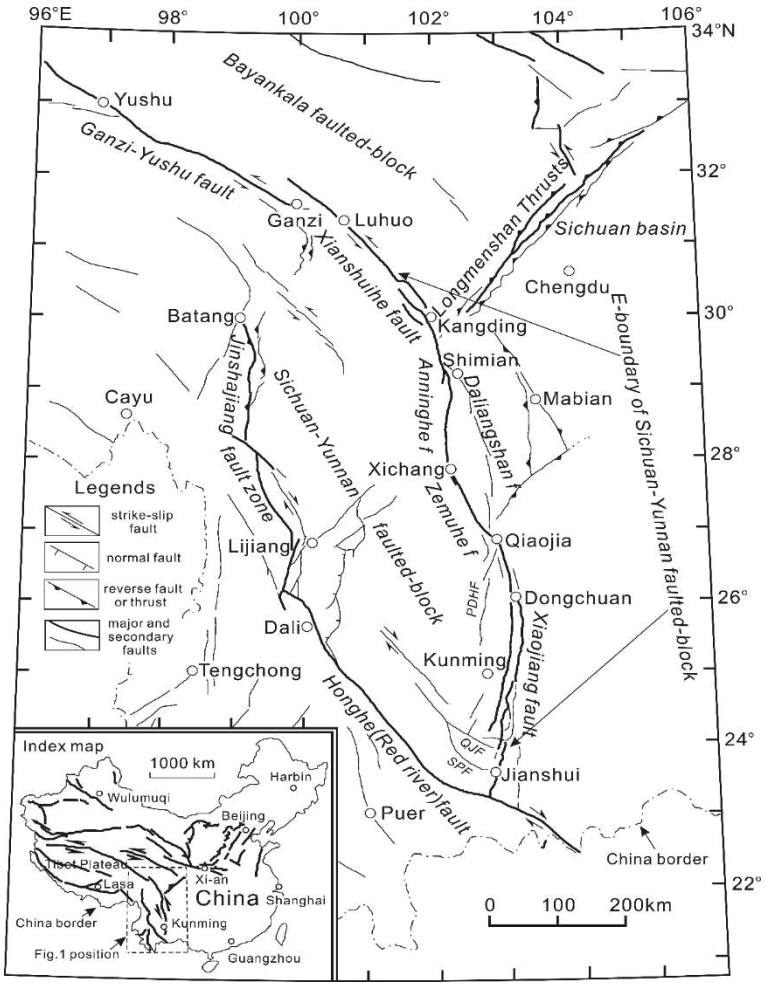

Fig. 1 A simplified map of active faults in and surrounding the Sichuan-Yunnan faulted-block of southwestern China (Wen et al. 2008). Index map shows the position of the Sichuan-Yunnan faulted-block in continental China. QJF, Qujiang fault; SPF, Shiping fault; PDHF, Puduhe fault

2. Data Acquisition and Processing

The strong-motion data used in this study were collected from CSMNC (see **Data Availability**). The selection of strong-motion recordings mainly adhered to the following criteria:

(1) Selecting the recordings collected from free-field stations, and non-free-field station recordings were removed.

(2) Excluding the recordings not in the Sichuan-Yunnan region.

(3) Recordings of obviously poor-quality were excluded following the visual inspection of the strong-motion recordings (for example, recordings with multiple wave packets, severe drop tail, spikes, noise-dominated recordings, and unreliable recordings).

(4) Recordings with incomplete two horizontal components were excluded.

(5) We did not use recordings with the source to site distance greater than 400 km (rupture distance for $M_w > 6$, and hypocentral distance for $M_w \leq 6$).

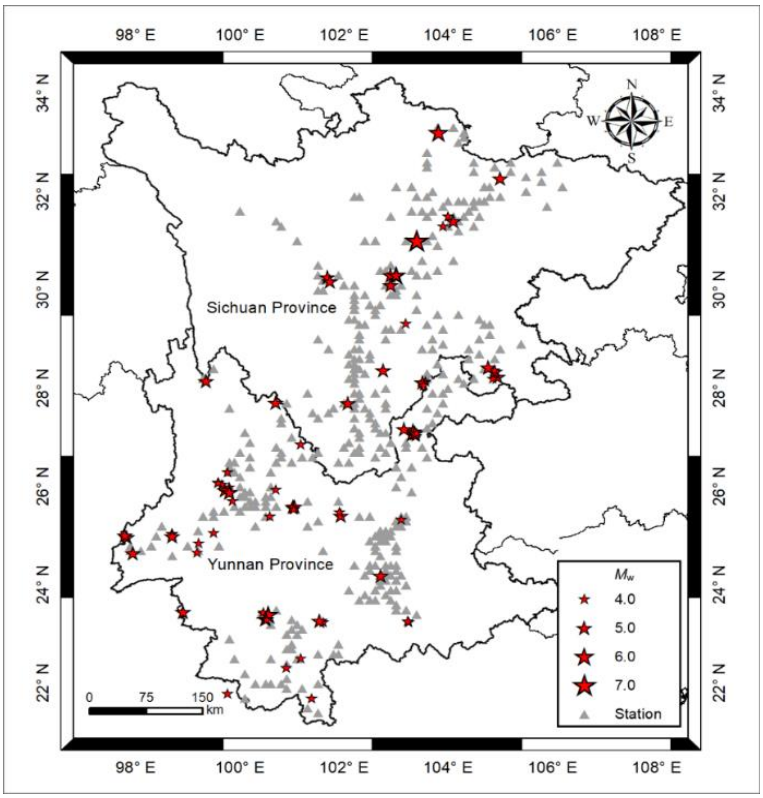

Fig. 2 Locations of earthquakes and strong-motion stations used in this study. Star indicates the epicenter, and triangle denotes the strong-motion station

The final dataset used in this study consists of 1605 recordings obtained at 491 stations from 78 earthquakes in the magnitude range of $4.2 \leq M_w \leq 7.9$ occurring from 2008 to 2020. Table 1 shows more detailed information about these earthquakes. The time, epicenter location, and focal depth were derived from uncorrected strong-motion recording data files. The moment magnitude (using the body-wave magnitude (M_b) for unknown focal mechanism) and fault type were determined from the focal mechanism solution provided by the U.S. Geological Survey (USGS, https://www.usgs.gov/, last accessed on January 31, 2021) and the Global Centroid Moment Tensor (GCMT, https://www.globalcmt.org/, last accessed on January 31, 2021). The provisions of the NGA-west2 project (https://ngawest2.berkeley.edu/, last accessed on January 5, 2021) were followed to classify the fault types by slip rake. In this classification, (1) SS represents strike-slip fault ($-180 < \text{Rake} < -150$, $-30 < \text{Rake} < 30$ and $150 < \text{Rake} < 180$); (2) N represents normal fault ($-120 < \text{Rake} < -60$); (3) R represents reverse fault ($60 < \text{Rake} < 120$); (4) RO represents reverse-oblique fault ($30 < \text{Rake} < 60$ and $120 < \text{Rake} < 150$); (5) NO represents a normal-oblique fault ($-150 < \text{Rake} < -120$ and $-60 < \text{Rake} < -30$); and (6) U (Unknown) represents unknown focal mechanism. Figure 2 shows the distribution of epicenters and stations used in the dataset, and it is obvious that these earthquakes concentrate in the fault zones within and surrounding the Sichuan-Yunnan faulted-block and the Longmenshan Thrusts zone (Fig. 1).

Table 1 Parameters of the earthquakes in the Sichuan-Yunnan region used in this study

Number	Date (yy-mm-dd)	Time (UTC+8)	Magnitude (M_w)	Longitude	Latitude	Depth (km)	Fault Type	Number of Records
1#	2008-05-12	14:28	7.9	103.400	31.000	14	R	119
2#	2009-06-30	02:03	5.3	104.100	31.400	20	R	9
3#	2009-06-30	15:22	4.9	104.000	31.500	20	R	7
4#	2009-11-28	00:04	4.9	103.900	31.300	21	R	3
5#	2013-04-20	08:02	6.8	103.000	30.300	13	R	83
6#	2013-04-20	08:07	5.1	102.900	30.300	10	R	32

7#	2013-04-20	11:34	5.4	102.900	30.100	11	R	52
8#	2013-04-21	04:53	4.8	103.000	30.300	16	R	53
9#	2013-04-21	17:05	5.2	103.000	30.300	17	R	52
10#	2014-10-01	09:23	5.2	102.760	28.370	15	SS	16
11#	2014-11-22	16:55	5.9	101.690	30.260	18	SS	55
12#	2014-11-25	23:19	5.7	101.730	30.180	16	SS	35
13#	2015-01-14	13:21	4.9	103.190	29.320	14	R	36
14#	2017-08-08	21:19	6.5	103.820	33.200	20	SS	66
15#	2017-09-30	14:14	5.1	105.000	32.270	13	RO	34
16#	2018-10-31	16:29	5	102.080	27.70	19	SS	45
17#	2018-12-16	12:46	5.3	104.950	28.240	12	SS	16
18#	2019-01-03	08:48	4.8	104.860	28.200	15	R	4
19#	2019-06-17	22:55	5.8	104.900	28.340	16	R	42
20#	2019-06-17	23:36	5.1	104.770	28.430	16	RO	17
21#	2019-06-18	07:34	4.7	104.890	28.370	17	R	16
22#	2019-06-22	22:29	5.3	104.770	28.430	10	R	21
23*	2009-04-14	04:37	4.9	99.790	25.989	10	NO	13
24*	2009-07-09	19:19	5.7	101.029	25.600	6	SS	69
25*	2009-07-10	17:02	5.2	101.050	25.600	10	SS	13
26*	2009-07-10	20:57	4.2	101.000	25.569	13	SS	11
27*	2009-07-13	00:01	4.9	101.040	25.540	10	R	4
28*	2009-11-02	05:07	4.9	100.690	25.940	10	SS	9
29*	2010-01-01	10:08	5.0(M_b)	99.760	26.299	11	U	13
30*	2010-02-25	12:56	5.2	101.940	25.420	20	SS	31
31*	2010-06-01	23:58	4.9	99.209	24.850	5	SS	8
32*	2011-03-10	12:58	5.5	97.949	24.649	10	SS	3
33*	2011-05-31	21:13	4.7	98.699	25.040	11	RO	7
34*	2011-06-20	18:16	5	98.690	25.049	10	R	11
35*	2011-08-09	19:50	5.1	98.699	25.000	11	SS	20
36*	2012-06-24	15:59	5.5	100.690	27.709	11	N	9
37*	2012-09-11	11:21	4.9	99.182	24.659	14	NO	4
38*	2013-02-20	13:01	4.7	101.599	23.250	15	SS	4
39*	2013-03-03	13:41	5.2	99.720	25.930	9	N	24
40*	2013-04-17	09:45	5.3	99.800	25.899	11	NO	24
41*	2013-08-31	08:04	5.6	99.349	28.149	10	N	6
42*	2013-11-28	16:23	4.8	100.580	25.399	10	N	9
43*	2014-01-15	03:17	4.8(M_b)	101.169	26.860	33	U	8
44*	2014-01-28	20:01	4.5(M_b)	101.169	22.510	7	U	16
45*	2014-04-05	06:40	4.9	103.569	28.139	13	RO	10
46*	2014-05-07	22:11	4.8	101.916	25.482	13	SS	9
47*	2014-05-24	04:49	5.8	97.830	24.979	12	SS	8
48*	2014-05-30	09:20	5.9	97.800	25.020	12	SS	11
49*	2014-08-03	16:30	6.2	103.330	27.110	10	SS	66
50*	2014-08-17	06:08	5.1	103.510	28.120	7	SS	26
51*	2014-10-07	21:49	6.1	100.550	23.399	10	SS	30
52*	2014-10-11	14:05	4.7	100.449	23.450	10	SS	3
53*	2014-12-06	02:43	5.6	100.489	23.319	10	SS	23
54*	2014-12-06	18:20	5.6	100.500	23.319	10	SS	23
55*	2014-12-07	17:23	4.6	100.510	23.299	16	SS	2
56*	2015-03-01	18:24	5.3	98.910	23.459	11	SS	13
57*	2015-03-09	17:59	4.8	103.099	25.329	12	SS	33
58*	2015-10-30	19:26	4.9	99.500	25.059	10	N	20
59*	2015-11-14	00:55	4.3	100.519	23.299	6	SS	4
60*	2016-02-08	07:30	4.6(M_b)	99.660	26.049	10	U	2
61*	2016-03-05	19:20	4.5(M_b)	101.379	21.700	10	U	11
62*	2016-05-04	15:51	4.5(M_b)	103.239	23.250	10	U	5
63*	2016-05-04	17:24	4.5(M_b)	103.220	23.270	10	U	3
64*	2016-05-18	00:48	5	99.583	26.082	17	SS	18
65*	2016-05-18	01:05	4.8	99.580	26.079	10	N	13
66*	2016-07-29	22:02	4.7(M_b)	99.760	21.799	30	U	11
67*	2016-08-12	14:56	4.7	103.370	27.030	13	SS	4

68*	2016-08-12	19:25	4.6	103.389	27.030	6	SS	4
69*	2016-11-17	12:22	4.5(M_b)	99.860	25.709	10	U	11
70*	2017-02-08	19:11	5.1	103.370	27.090	10	SS	8
71*	2017-03-12	20:21	4.8	103.400	27.090	10	SS	7
72*	2017-03-27	07:40	5	99.809	25.870	10	SS	13
73*	2017-03-27	07:55	5.1	99.800	25.889	12	SS	16
74*	2018-02-09	22:58	4.6(M_b)	100.889	22.319	12	U	12
75*	2018-08-13	01:44	5.1	102.709	24.190	7	SS	42
76*	2018-09-08	10:31	5.7	101.529	23.280	11	SS	36
77*	2019-05-16	04:33	4.8	103.529	28.069	10	SS	5
78*	2020-05-18	21:47	5.1	103.160	27.180	8	N	20

Earthquakes in Sichuan province

* Earthquakes in Yunnan province

The V_{s30} (the average shear-wave velocity in the upper 30 meters of a soil profile) is a popular parameter for expression of site effects in attenuation relationships (e.g. Anderson et al. 1996; Castro et al. 1997; Park and Elrick 1998; Anderson et al. 1996; Lee et al. 2012). The V_{s30} values of all stations in this dataset were not directly measured from the shear wave velocity profile. Instead, the V_{s30} values of approximately half of the stations were derived from the literature (Yu and Li 2015; Zhang et al. 2020) and the NGA-West2 database flat file (https://peer.berkeley.edu, last accessed on January 5, 2021). For other sites where the shear wave velocity is available (Li et al. 2013; Zhao et al. 2019) according to the 2010 seismic design code (Chinese Standard 2008), the V_{s30} values were calculated by Eqs. 1 modified from Wang et al. (2010). For sites without borehole information, the V_{s30} values were inferred from geological units, considering such factors as geotechnical category, terrain-based categories, etc.

$$V_{s30} = \begin{cases} 30 \Big/ \left[d/V_{se} + (30-d)/500 \right] & \text{for } d \le 30 \text{ m} \\ V_{se} & \text{for } d > 30 \text{ m} \end{cases} \quad (1)$$

where d is the depth to the rock, in m and V_{se} is the equivalent shear wave velocity (the average shear-wave velocity of the soil layers in the top 20 m or the soil above rock for sites with d less than 20 m), in m/s.

Figure 3 shows the distribution of magnitudes, distances, and V_{s30} values of these recordings. The dataset includes recordings having moment magnitudes ranging between 4.2 and 7.9, distances ranging between 0.481 and 396.29 km, and V_{s30} values ranging between 128 and 760 m/s (according to the National Earthquake Hazards Reduction Program (NEHRP) site classification standard (BSSC 1994)). Most of the recording stations belong to class C and class D sites, and 6 stations belong to class E sites.

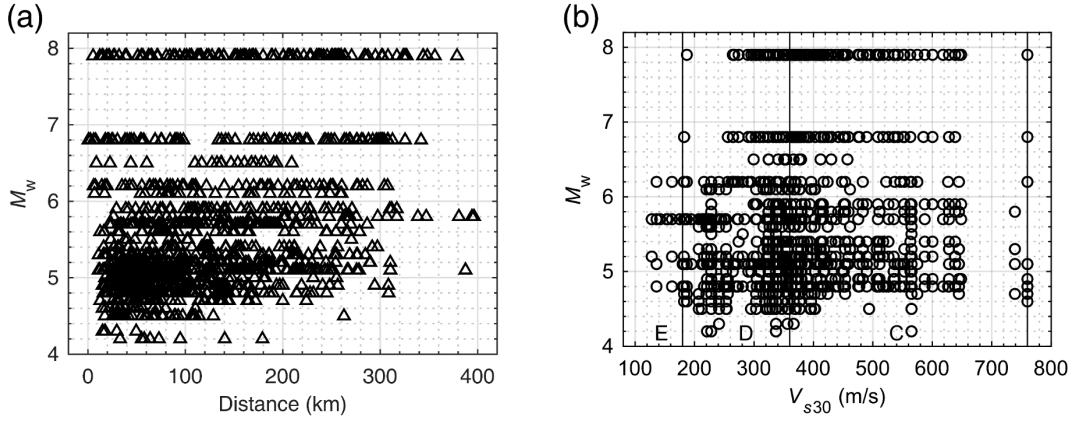

Fig. 3 Magnitude, distance, and V_{s30} distribution of strong-motion data selected in the present study: magnitude with (a) distance and (b) V_{s30}

The Arias intensity formula selected for this study is the average of the Arias intensity from two

perpendicular horizontal components, as expressed in Eqs. 2:

$$I_a = \frac{I_{xx} + I_{yy}}{2} \tag{2}$$

where I_{xx} and I_{yy} are the Arias intensities from two perpendicular horizontal components.

3. Predictive attenuation relation for Arias intensity

The Arias intensity attenuation relationship form used in this study is modified from Lee et al. (2012) as follows:

$$\ln I_a = c_1 + c_2(M-6) + c_3 \ln(M/6) + c_4 \ln(R + c_5) + c_6 \ln(V_{s30}/500) + c_7 F_N + c_8 F_R + \eta + \varepsilon \tag{3}$$

where I_a is the average of the Arias intensity from two horizontal components, in m/s, M is the moment magnitude, R is the source to site distance (the closest distance to the rupture plane (rupture distance) for large earthquakes ($M_w > 6$) and hypocentral distance for others ($M_w \leq 6$), in km), V_{s30} is the average shear wave velocity of 30 meters on the soil profile, in m/s, F_N and F_R are dummy variables indicating the fault types ((1, 0) for normal and normal-oblique faults, (0, 1) for reverse and reverse-oblique faults, (0,0) for other (strike-slip and unknown faults)), η are the inter-event residuals conforming to the normal distribution of N(0, ϕ^2); ε are the intra-event residuals conforming to the normal distribution of N(0, τ^2); $c1$, $c2$, …, $c8$ are regression coefficients. Eqs. 4 determine the total standard deviation σ.

$$\sigma = \sqrt{\phi^2 + \tau^2} \tag{4}$$

The regression algorithm described by Joyner and Boore (1993) was used in the regression analysis of Eqs. 3.

4. Results and Evaluations

After using the regression analysis mentioned above, the median Arias intensity attenuation relationship is expressed as:

$$\ln I_a = 3.190 + 4.553(M-6) - 15.487 \ln(M/6) - 2.140 \ln(R+3) - 0.643 \ln(V_{s30}/500) - 0.456 F_N + 0.901 F_R \tag{5}$$

All variables were determined as previously defined. The inter-event standard deviation ϕ is 0.852 (in natural log format), the intra-event standard deviation τ is 1.270 (in natural log format), and the total standard deviation σ consisting of ϕ and τ is 1.529 (in natural log format).

In Eqs. 5, the negative value for F_N means that the Arias intensity of the normal (including normal-oblique) event is 0.456 (in natural log format) smaller than that of the strike-slip event. The positive value for F_R means that the Arias intensity of the reverse (including reverse-oblique) event is 0.901 (in natural log format) larger than that of the strike-slip event. The Arias intensity attenuation curves for different magnitudes and fault styles (Fig. 4) show the same trends with Eqs. 5, indicating effects of focal mechanism, which is consistent with other previous research (e.g. Travasarou et al. 2003; Stafford et al. 2008; Foulser-Piggott and Stafford 2012; Lee et al. 2012; Foulser-Piggott and Goda 2015; Campbell and Bozorgnia 2019).

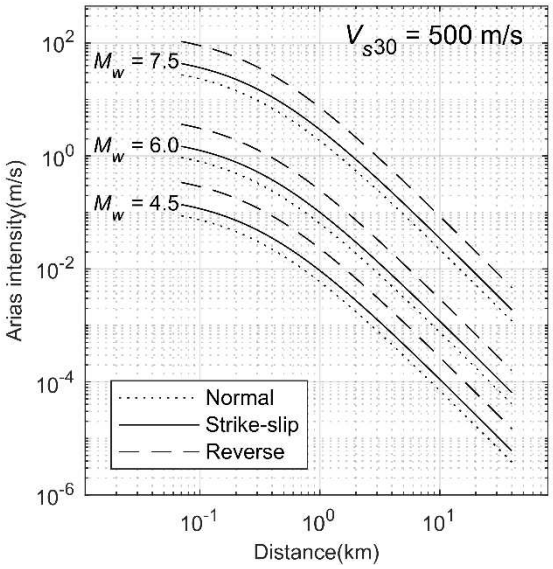

Fig. 4 Arias intensity attenuation curves obtained by this study for different magnitudes and fault styles

As shown in Figure 5, the Arias intensity in softer sites (sites with V_{s30} = 280 m/s) is higher than that in harder sites (sites with V_{s30} = 560 m/s). The $c5$ for V_{s30} in Eqs. 5 is negative and reflects the same trend, indicating the site effects on Arias intensity, which is consistent with the conclusions regarding site effects using V_{s30} of other previous studies (e.g. Lee et al. 2012; Campbell and Bozorgnia 2012; Foulser-Piggott and Goda 2015; Campbell and Bozorgnia 2019; Bahrampouri et al. 2020).

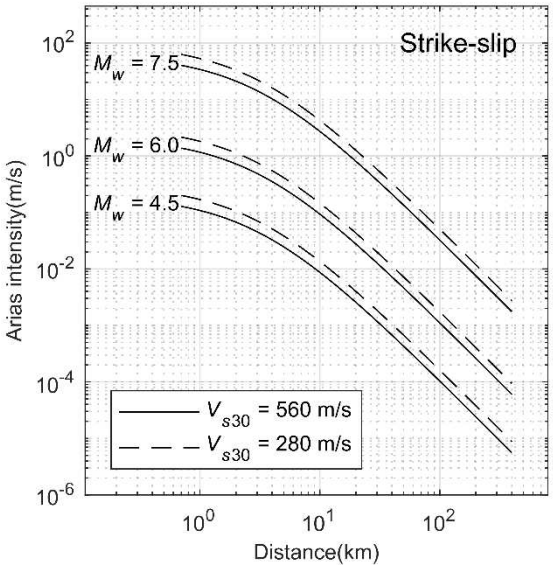

Fig. 5 Arias intensity attenuation relationship obtained by this study for different magnitudes and V_{s30}

Figure 6 shows the median attenuation curves and data distributions of several typical earthquakes in the Sichuan-Yunnan region (including the Wenchuan (2008.5.12, M_w 7.9 reverse event) in Figure 6a, the Lushan (2013.4.20, M_w 6.8 reverse event) in Figure 6b, the Jiuzhaigou (2017.8.8, M_w 6.5 strike-slip event) in Figure 6c, the Ludian (2014.8.3, M_w 6.2 strike-slip event) in Figure 6d, the Gongxian (2019.6.17, M_w 5.1 reverse-oblique event) in Figure 6e, and the Qiaojia (2020.5.18, M_w 5.1 normal event) in Figure 6f). It is observed that the attenuation curve obtained in this study fits the distribution of the Arias intensity of earthquakes in the Sichuan-Yunnan region well.

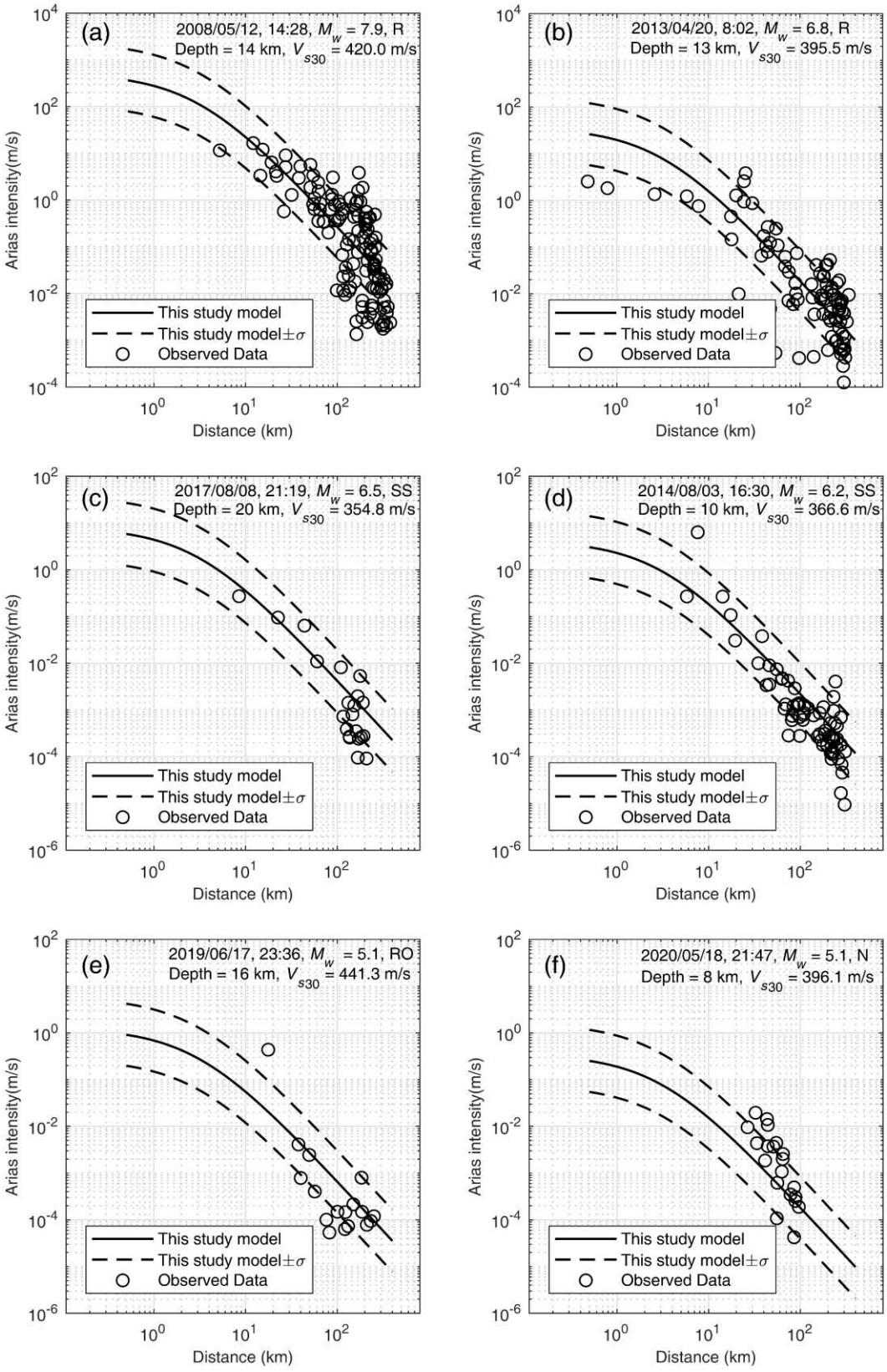

Fig. 6 Fit of the median and one sigma Arias intensity attenuation curve to the data for (a) 2008 Wenchuan reverse earthquake, (b) 2013 Lushan reverse earthquake, (c) 2017 Jiuzhaigou strike-slip earthquake, (d) 2014 Ludian strike-slip earthquake, (e) 2019 Gongxian reverse-oblique earthquake, and (f) 2020 Qiaojia normal earthquake

Several models were selected for shallow earthquakes with the same consideration factors (e.g.

fault types, site effect, etc.) as the comparative models for this study, including Travasarou et al. 2003 (Tra03), Hwang et al. 2004 (Hwa04), Stafford et al. 2009 (Sta09), F. − P. & Stafford 2012 (FPS12), and Lee et al. 2012 (Lee12). As noted, the Z_{HYP} (focus depth) in Sta09 is determined by the relation with M_w (Scherbaum et al. 2004). Figure 7 compares this study's median attenuation curve (strike-slip event, V_{s30} = 280 m/s or class D sites) with the comparative models. For the large event (M_w = 7.5), the estimated value at near sites (R < 10 km) for this study is slightly larger than that of FPS12 and much larger than those of other comparative models. The estimated value in the sites of R > 10 km of this study is smaller than that of Hwa04 (the gap increasing with distance) and minimally different from those of other comparative models (Fig. 7a). For the middle event (M_w = 6), the estimated value of this study model at the near sites (R < 10 km) is larger than those of other models (except Sta09 and FPS12 in sites of 1 km < R <10 km). The estimated value in the sites of R > 10 km of this study is smaller than those of Tra03 and Hwa04 (the gap increasing with distance) and also smaller than those of Sta09 (the gap decreasing with distance). The estimated value of this study is minimally different than those of FPS12 and Lee12 (Fig. 7b). For the small event (M_w = 4.5), there is an intersection at the distance of 70 km in the curves of this study, Tra03, Hwa04, and Sta09, and the estimated value of this study is always larger than those of FPS12 and Lee12 for the entire distance range (Fig. 7c). The above comparison indicates that there are noticeable differences between this study model and the comparative models (the comparison of normal and reverse events as Fig. 13,14 in **Appendix**). The differences in the near sites may primarily be due to, the datasets being derived from differing regions. The differences in the middle- and far-fields may be partly due to the difference in characteristics of the datasets, and partly, the difference in slopes of the attenuation curves related to Q values.

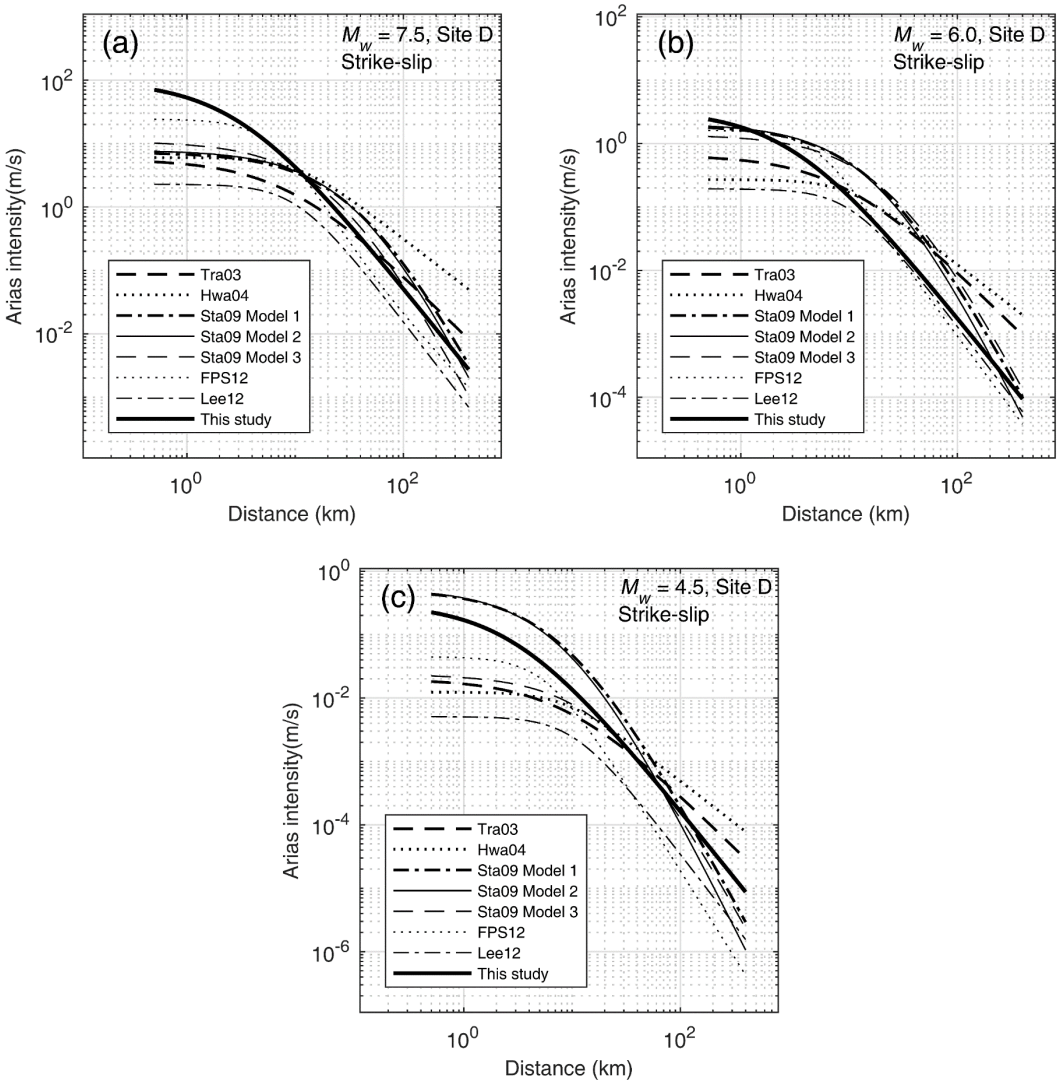

Fig. 7 Comparison for distance scaling of attenuation equations between this study and previous studies for strike-slip event in Class D site

5. Uncertainty analysis

Figure 8 shows the distributions of intra-event residuals with V_{s30}, distance, and earthquake magnitude. The V_{s30}-binned means of intra-event residuals show a slightly decreasing trend with V_{s30} (Fig. 8a), probably representing the nonlinear site effects. There is no systematic trend in intra-event residuals with distance (Fig. 8b) and earthquake magnitude (Fig. 8c). The intra-event residuals obey a log-normal distribution (Fig. 8d).

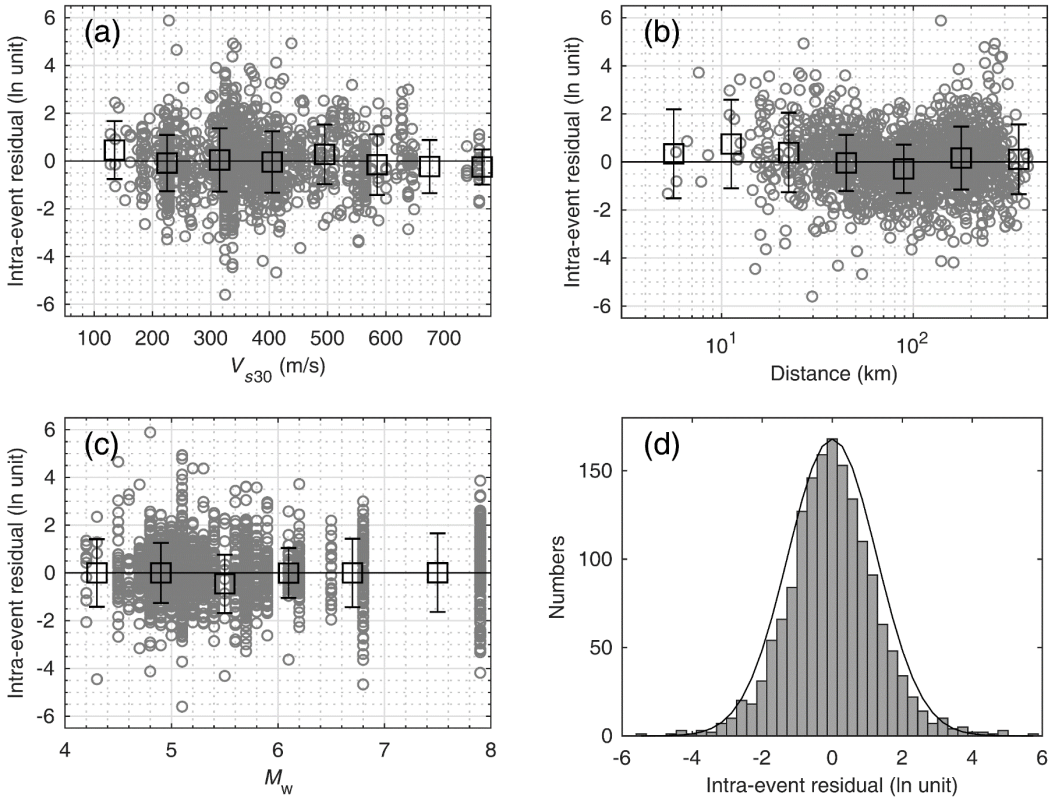

Fig. 8 Distribution of intra-event residuals with different parameters: (a) V_{s30}, (b) distance, and (c) earthquake magnitude. (d) Histogram of intra-residuals and its fit to a normal distribution curve. Box and error bar denotes the mean ± one standard deviation of binned intra-event residuals

The distribution of inter-event residuals with earthquake magnitude is shown in Figure 9. There is no obvious trend of inter-event residuals for reverse (including reverse-oblique), normal (including normal-oblique), or strike-slip earthquakes. The positive values of inter-event residuals for most unknown earthquakes indicate the possibility of reverse events. The dispersion of inter-event residuals for small and moderate events is noticeably stronger than for large events. As a result, the inter-event standard deviation of this study is 0.852, which is larger than those of the other comparative models noted earlier. One possible explanation may be the different source effects derived from the complicated seismotectonic activities in the Sichuan-Yunnan region (Fig. 1).

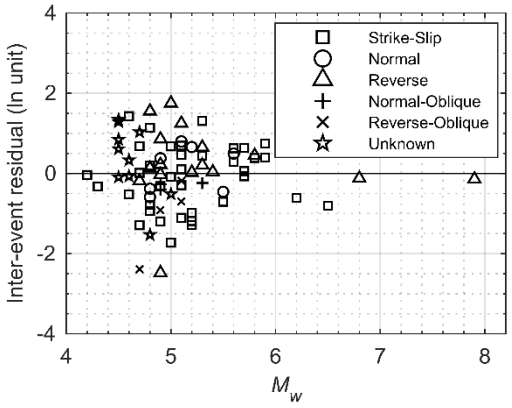

Fig. 9 Distribution of inter-event residuals with earthquake magnitude

The total standard deviation σ in this study (1.529) is larger than that of Tra03 (1.328), larger than

that of Hwa04 (1.290, 1.230, 1.250, and 0.820 in class B, C, D, and E sites, respectively), larger than that of Sta09 (0.973 (form 1), 0.952 (form 2) and 1.019 (form 3) in soil sites; 1.153 (form 1), 1.138 (form 2) and 1.170 (form 3) in rock sites), larger than that of FPS12 (1.171), and larger than that of Lee12 (0.994). In addition to the inter-event standard deviation analyzed above, the intra-event standard deviation of this study is 1.270, contributing significantly to the total standard deviation.

The intra-event residuals ε could be further decomposed into inter-site (site-to-site) residuals ε_s and remain residuals ε_r. The intra-event standard deviation τ could also be decomposed into inter-site standard deviation τ_s and the remainder τ_r (Chen and Tsai, 2002). The ε_s reflects the site effects in station s can be estimated as:

$$\varepsilon_s = \frac{1}{n_{es}} \sum_{i=1}^{n_{es}} \varepsilon_i \qquad (6)$$

where n_{es} is the number of earthquakes recorded by station s, ε_i is the intra-event residual of the i th earthquake in station s.

The inter-site standard deviation τ_s can be expressed as follows:

$$\tau_s = \sqrt{\frac{1}{n_s} \sum_{s=1}^{n_s} \varepsilon_s^{\,2}} \qquad (7)$$

where n_s is the number of stations.

This dataset consists of 1605 recordings obtained at 491 stations, and most stations have only a few recordings. The inter-site residuals of those stations have no statistical meaning. Nineteen stations with more than 10 recordings each were selected, with the distribution of inter-site residuals calculated by Eqs. 6 with V_{s30} is shown in Figure 10. The decreasing trend of the inter-site residuals with estimated V_{s30} indicates substantial nonlinear site effects. Due to the error from inferring V_{s30}, the inter-site residuals of some sites are biased very heavily (e.g. 2.040 in 53YPX station, −0.635 in 53DFD station, etc.). As a result, there is an insignificantly decreasing trend of inter-site residuals in inferred V_{s30} sites. The inter-site standard deviation, which was calculated according to Eqs. 7, peaked at 0.603, indicating an outstanding contribution to intra-event standard deviation. We note that many of the stations are located in the Sichuan basin and the intermountain basin. Thus, the basin effects are another potential factor contributing to intra-event standard deviation.

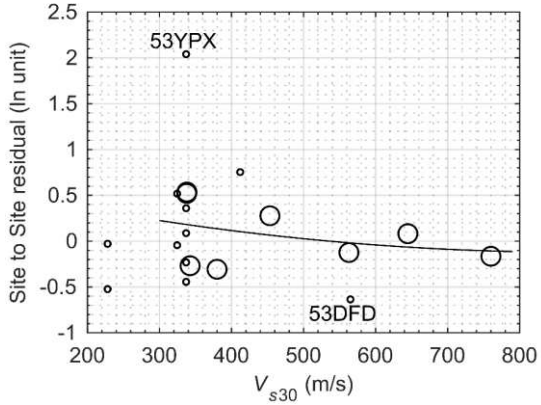

Fig. 10 The inter-site residuals against V_{s30}. The big circles and curve represent inter-site residuals of estimated V_{s30} sites (having shear wave velocity information in **Data Acquisition and Processing**) and fit curve of them; the small circles represent inter-site residuals of inferred V_{s30} sites (no shear wave velocity information in **Data Acquisition and Processing**)

After the Wenchuan M_w 7.9 earthquake, the damage investigation showed more earthquake-induced landslides in the hanging wall than the foot wall (Xu and Li, 2008), likely indicating the hanging wall effect on Arias intensity for large earthquakes. Following the criteria of the hanging wall effect found by Abrahamson and Silva 2008 (M_w > 6, dip < 70, $|R_x|$ <50 km (R_x, the horizontal distance to the top edge of the rupture measured perpendicular to strike, positive value for hanging wall and negative value for foot wall), and R_{jb} <30 km (R_{jb}, Horizontal distance to the surface projection of the rupture)), hanging wall effect recordings were selected. Figure 11 shows the distribution of intra-event residuals of selected recordings with R_x. There is no obvious difference between the hanging and foot wall. The mean of intra-event residuals of hanging wall is −0.360, while that of foot wall is −0.321, indicating insignificant hanging wall effect on Arias intensity in the Sichuan-Yunnan region. Thus, the development of landslides of the Wenchuan earthquake in the hanging wall is likely related to other factors (e.g. hanging wall effect on PGA, etc.).

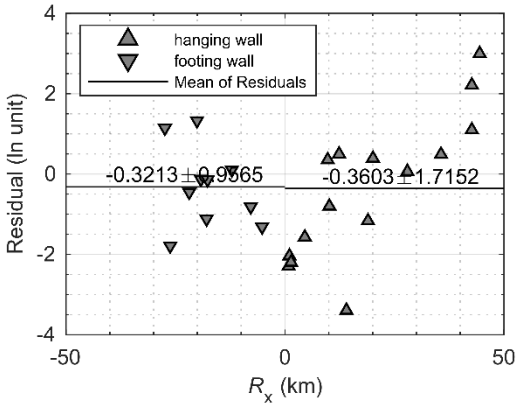

Fig. 11 Distribution of intra-event residuals with R_x and binned means of hanging wall and foot wall

6. Model prediction Test

On May 21, 2021 (Beijing time (UTC+8) 21:48:37), an earthquake occurred in Yangbi county (25.67°N, 99.87°E) in the northwest of Yunnan Province. According to the focal mechanism solution provided by USGS, the earthquake was a strike-slip earthquake with M_w 6.1 (https://www.usgs.gov/, last accessed on May 31, 2021). The predictive accuracy of this study model was tested using the strong-motion data of the Yangbi earthquake (25 recordings).

The goodness-of-prediction of the median attenuation curves of this study to the Yangbi earthquake data is shown in Figure 12a. Compare to the current study (Fig. 12b), other models have the tendency of underprediction (Fig. 12c,d) or overprediction (Fig. 12e) of the data from the Yangbi earthquake.

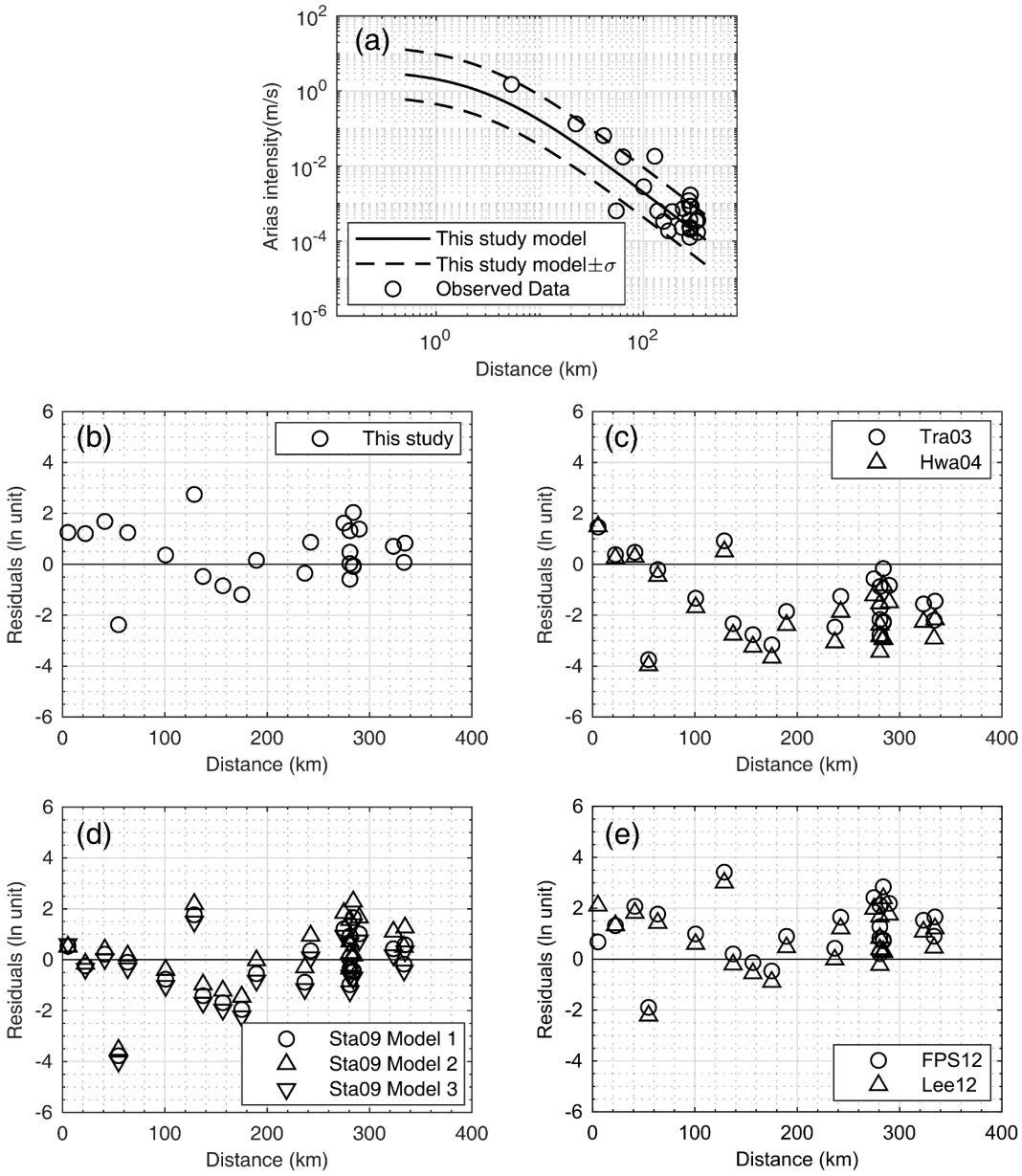

Fig. 12 (a) Prediction of the median and one sigma Arias intensity attenuation curve of this study and observed data in Yangbi earthquake. Distribution of the predicted residuals of (b) this study, (c) Tra03, Hwa04, (d) Sta09, (e) FPS12 model, and Lee12 model with distance

$$\Delta_s = \ln I_{as} - \ln \overline{I_{as}} \tag{8}$$

where Δ_s is the predicted residuals for site s, $\ln I_{as}$ is the natural log of observed Arias intensity for site s, $\ln \overline{I_{as}}$ is the natural log of predicted Arias intensity for site s.

For comparison of the prediction results quantitatively, we introduced the root mean square error (RMSE) as follows:

$$\mathrm{RMSE} = \sqrt[2]{\frac{\sum_1^n \Delta_s^{\,2}}{n}} \tag{9}$$

where Δs is the predicted residuals for site s, and n is the number of recordings.

A smaller RMSE denotes a higher predictive accuracy. The RMSE values of different models

based on the Yangbi earthquake data are shown in Table 2. The RMSE of this study model is 1.203, the lowest of all models, indicating that this study model has the highest accuracy in predicting the data of the Yangbi earthquake.

Table 2 Root mean square error (RMSE) of different models based on the Yangbi earthquake data

Model	Tra03	Hwa04	Sta08-1	Sta08-2	Sta08-3	FPS12	Lee12	This study
RMSE	1.901	2.361	1.206	1.282	1.276	1.580	1.386	1.203

7. Conclusions

This study has developed a region-specific Arias intensity attenuation relationship for the shallow earthquakes in the Sichuan-Yunnan region using 1605 recordings from 78 earthquakes recorded by 491 stations from 2008 to 2020. The relationship formula is modified from Lee et al. (2012), considering source (magnitude and focal mechanism), path, and site effects. As with previous studies, the strong effects of focal mechanism and site category on Arias intensity were found in this study. However, hanging wall effects were found to be insignificant. The total standard deviation of this relationship is 1.529, which is larger than found in previous studies and likely caused by the complicated seismotectonic activities, the nonlinear site effects, the error from inferring V_{s30}, the basin effects, and other possible factors. Development of a robust relationship would be proposed by using a constantly updated and more reliable database in the future.

Our comparisons with similar models for other regions indicate significant differences in Arias intensity (Fig. 7,13,14). However, the accuracy of the output of this relationship relative to the data in the Sichuan-Yunnan region and the highest predictive accuracy of this relationship to the data of Yangbi earthquake in Yunnan province demonstrate the best performance in modeling and prediction for this region. Thus, we consider this relationship to be valid in the Sichuan-Yunnan region for moment magnitudes ranging between 4.2 and 7.9, distances ranging between 0 and 400 km, and V_{s30} ranging between 128 and 760 m/s. This relationship may only provide a reference for the shallow earthquakes in the Sichuan-Yunnan region and the other regions with similar seismotectonic settings. Thus, it should be used carefully in other settings.

Acknowledgments We extend our deepest thanks to the Institute of Engineering Mechanics, China Earthquake Administration (CEA), for providing the strong-motion data. This research was supported by the National Natural Science Foundation of China (Grant number: 51808444).

Author contributions All authors contributed to the study conception and design. Data collection and analysis were performed by all authors.

Funding This research was supported by the National Natural Science Foundation of China (Grant number: 51808444).

Data Availability Strong-motion data used in this research were provided by the CSMNC (http://www.csmnc.net/, last accessed December 2020) operated by Institute of Engineering Mechanics, CEA. Please note that this website is currently under maintenance. During this period, please get in touch with the official e-mail csmnc@iem.ac.cn for data application. The V_{s30} values were partly obtained from the Next Generation Attenuation-West 2 (NGA-West2) site database (https://peer.berkeley.edu, last accessed on January 5, 2021). The focal mechanisms were obtained from USGS (https://www.usgs.gov/, last accessed on May 31, 2021) and GCMT (https://www.globalcmt.org/, last accessed on May 31, 2021). The datasets generated during the current study are available from the corresponding author on reasonable request.

Declarations

Conflicts of interest There is no conflict of interest/competing interest.

Appendix

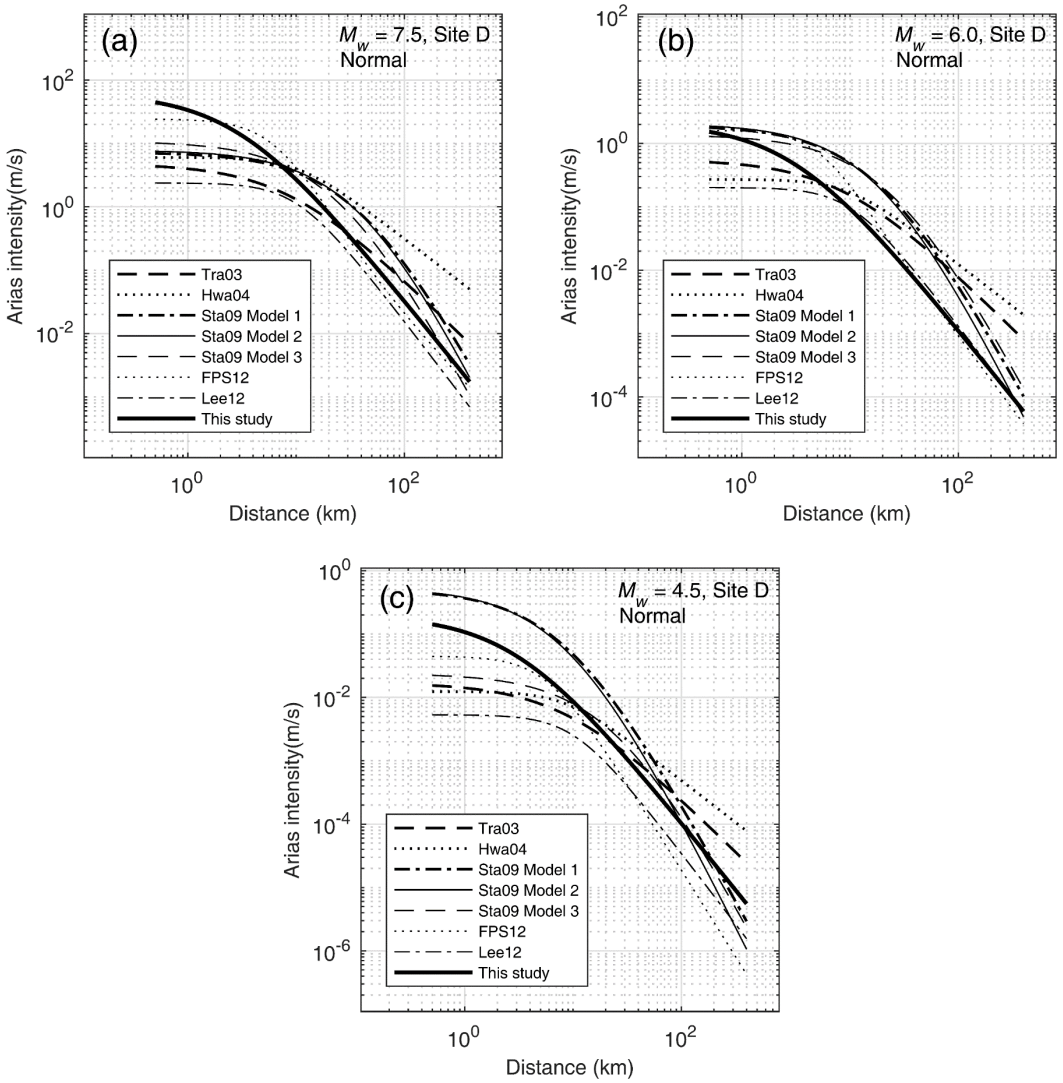

Fig. 13 Comparison for distance scaling of attenuation equations between this study and previous studies for normal event in Class D site

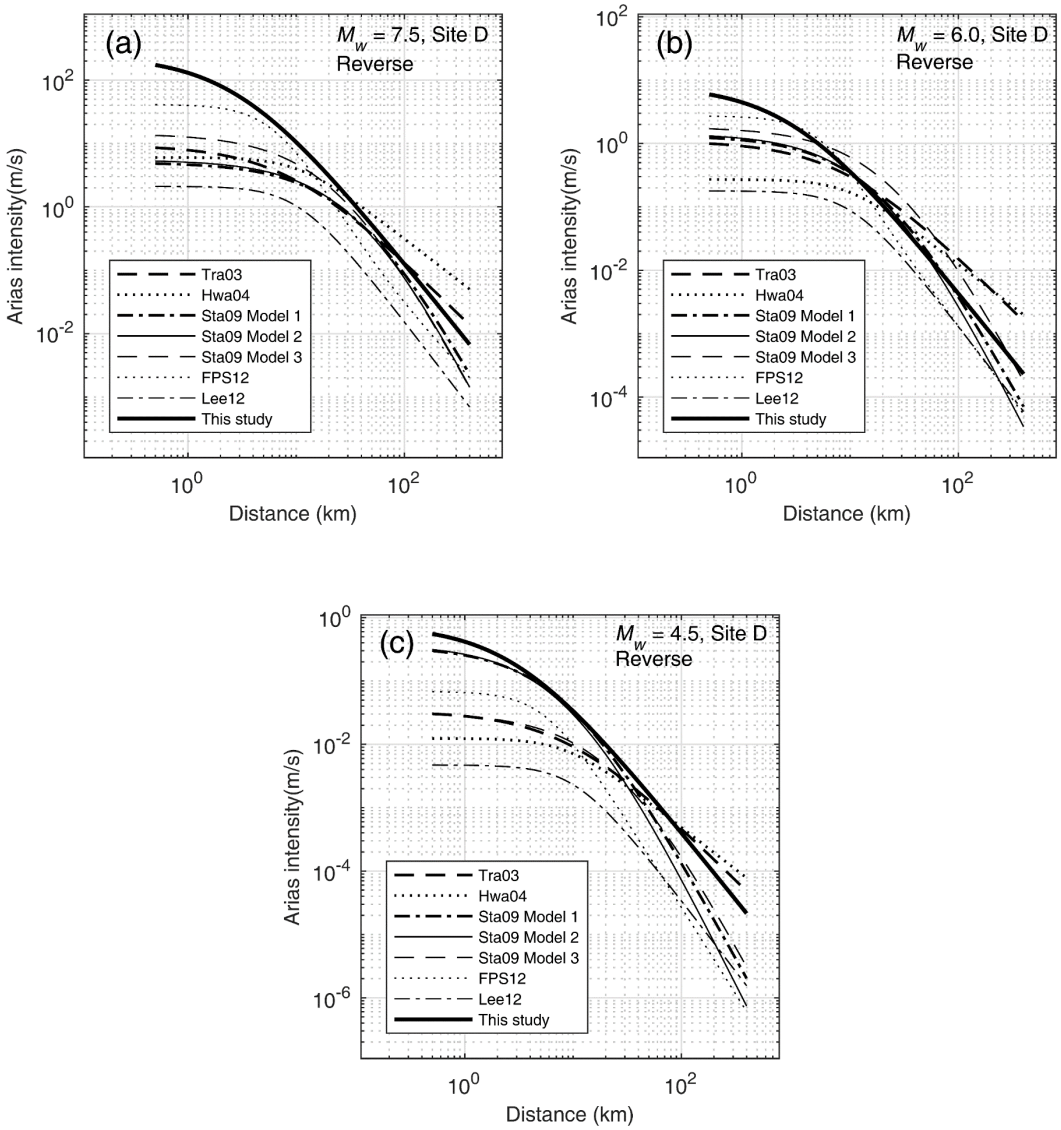

Fig. 14 Comparison for distance scaling of attenuation equations between this study and previous studies for reverse event in Class D site

References

Allen CR, Luo Z, Qian H, Wen X, Zhou H, Huang W (1991) Field study of a highly active fault zone: the Xianshuihe fault of southwestern China. Geol Soc Am Bull 103(9):1178-1199. https://doi.org/10.1130/0016-7606(1991)103<1178:FSOAHA>2.3.CO;2

Arias A (1970) A measure of earthquake intensity, In: Hansen RJ (ed), Seismic design for nuclear power plants, MIT Press, Cambridge, Massachusetts, pp 438-483.

Anderson JG, Lee Y, Zeng Y, Day S (1996) Control of strong motion by the upper 30 meters. Bull Seismol Soc Am 86(6):1749-1759. https://doi.org/10.1785/BSSA0860061749

Bahrampouri M, Rodriguez-Marek A, Green RA (2020) Ground motion prediction equations for Arias intensity using the Kik-net database. Earthq Spectra 37(1):428-448. https://doi.org/10.1177/8755293020938815

Building Seismic Safety Council (BSSC) (1994) 1994 Edition, NEHRP recommended provisions for seismic regulations for new buildings, FEMA 222A, Part 1(Provisions): developed for the Federal Emergency Management Agency, Washington, DC

Campbell KW, Bozorgnia Y (2012) A comparison of ground motion prediction equations for Arias intensity and cumulative absolute velocity developed using a consistent database and functional form. Earthq Spectra 28(3):931-941. https://doi.org/10.1193/1.4000067

Campbell KW, Bozorgnia Y (2019) Ground motion models for the horizontal components of Arias intensity (AI) and cumulative absolute velocity (CAV) using the NGA-West2 database. Earth Spectra 35(3):1289-1310. https://doi.org/10.1193/090818EQS212M

Castro RR, Mucciarelli M, Pacor F, Petrungaro C (1997) S-wave site-response estimates using horizontal-to-vertical spectral rations. Bull Seismol Soc Am 87(1):256-260. https://doi.org/10.1785/BSSA0870010256

Chen YH, Tsai CP (2002) A new method for estimation of the attenuation relationship with variance components. Bull Seismol Soc Am 92(5):1984-1991. https://doi.org/10.1785/0120010205

Chousianitis K, Del Gaudio V, Kalogeras I, Ganas A (2014) Predictive model of Arias intensity and Newmark displacement for regional scale evaluation of earthquake-induced landslide hazard in Greece. Soil Dyn Earthq Eng 65:11-29. https://doi.org/10.1016/j.soildyn.2014.05.009

Foulser-Piggott R, Stafford PJ (2012) A predictive model for Arias intensity at multiple sites and consideration of spatial correlations. Earthq Eng Struct Dyn 41(3):431-451. https://doi.org/10.1002/eqe.1137

Foulser-Piggott R, Goda K (2015) Ground‐motion prediction models for Arias intensity and cumulative absolute velocity for Japanese earthquakes considering single‐station sigma and within‐event spatial correlation. Bull Seismol Soc Am 105(4):1903-1918. http://dx.doi.org/10.1785/0120140316

Hwang H, Lin CK, Yeh YT, Cheng SN, Chen KC (2004) Attenuation relations of Arias intensity based on the Chi-Chi Taiwan earthquake data. Soil Dyn Earthq Eng 24(7):509-517. https://doi.org/10.1016/j.soildyn.2004.04.001

Joyner WB, Boore DM (1993) Methods for regression analysis of strong-motion data. Bull Seismol Soc Am 83(2):469-487. https://doi.org/10.1785/BSSA0830020469

Lee CT, Hsieh BS, Sung CH, Lin PS (2012) Regional Arias intensity attenuation relationship for Taiwan considering VS30. Bull Seismol Soc Am 102(1):129-142. https://doi.org/10.1785/0120100268

Li ZG, Cui JW, Zhao YX, Shen K, Liu F (2013) Site characteristic analyses for strong earthquake networks in southern and southwestern Yunnan. J Seimol Res 36(4):508-513. (**in Chinese with English abstract**)

Liu JM, Gao MT, Xie JJ (2015) Spatial variability and attenuation of Arias intensity during the 1999 Chi‐Chi Mw 7.6 Earthquake, Taiwan. Bull Seismol Soc Am 105(3):1768-1778. https://doi.org/10.1785/0120140157

Liu JM, Wang T, Wu SR, Gao MT (2016) New empirical relationships between Arias intensity and peak ground acceleration. Bull Seismol Soc Am 106(5):2168-2176. https://doi.org/10.1785/0120150366

Lu Y, Li B, Xiong F, Dai K, Liu Y, Mei Z (2019) Bi-normalized Newmark-Hall spectra for seismic design and assessment. Bull Earthq Eng 17(11):5791-5807. https://doi.org/10.1007/s10518-019-00712-2

Park S, Elrick S (1998) Predictions of shear-wave velocities in southern California using surface geology. Bull Seismol Soc Am 88(3):677-685. https://doi.org/10.1785/BSSA0880030677

Rajabi AM, Khamehchiyan M, Mahdavifar MR, Del Gaudio V (2010) Attenuation relation of Arias intensity for Zagros Mountains region (Iran). Soil Dyn Earthq Eng 30(3):110-118. https://doi.org/10.1016/j.soildyn.2009.09.008

Sandıkkaya MA, Akkar S (2017) Cumulative absolute velocity, Arias intensity and significant duration predictive models from a pan-European strong-motion dataset. Bull Earthq Eng 15(5):1881-1898. https://doi.org/10.1007/s10518-016-0066-6

Scherbaum F (2004) On the conversion of source-to-site distance measures for extended earthquake source models. Bull Seismol Soc Am 94(3):1053-1069. http://dx.doi.org/10.1785/0120030055

Stafford PJ, Berrill JB, Pettinga JR (2009) New predictive equations for Arias intensity from crustal earthquakes in New Zealand. J Seismol 13(1):31-52. https://doi.org/10.1007/s10950-008-9114-2

Standard C (2008) Code for seismic design of buildings (GB 50011-2010). Chinese Building Press, Beijing

Tapponnier P, Molnar P (1977) Active faulting and tectonics in China. J Geophy Res 82(20):2905-2930. https://doi.org/10.1029/JB082i020p02905

Tapponnier P, Peltzer G, Le Dain AY, Armijo R, Cobbold P (1982) Propagating extrusion tectonics in Asia: new insights from simple experiments with plasticine. Geology 10(12):611-616. https://doi.org/10.1130/0091-7613(1982)10<611:PETIAN>2.0.CO;2

Travasarou T, Bray JD, Abrahamson NA (2003) Empirical attenuation relationship for Arias intensity. Earthq Eng Struct Dyn 32(7):1133-1155. https://doi.org/10.1002/eqe.270

Wang D, Xie LL, Abrahamson NA, Li SY (2010) Comparison of strong ground motion from the Wenchuan, China, earthquake of May 12 2008 with the Next Generation Attenuation (NGA) ground-motion models. Bull Seismol Soc Am 100(5B):2381–2395. https://doi.org/10.1785/0120090009

Wang T, Liu J, Shi J, Wu S (2017) The influence of DEM resolution on seismic landslide hazard assessment based upon the Newmark displacement method: a case study in the loess area of Tianshui, China. Environ Earth Sci 76(17): article number 604. https://doi.org/10.1007/s12665-017-6944-7

Wang Y, Song C, Lin Q, Li J (2016) Occurrence probability assessment of earthquake-triggered landslides with Newmark displacement values and logistic regression: The Wenchuan earthquake, China. Geomorphology 258:108-119. https://doi.org/10.1016/j.geomorph.2016.01.004

Wen X, Du P, Long D (2000) New evidence of paleoearthquakes and date of the latest event on the Xiaoxiangling mountain segment of the Anninghe fault zone. Seismol Geol 22:1-8. (**in Chinese with English abstract**)

Wen XZ, Ma SL, Xu XW, He YN (2008) Historical pattern and behavior of earthquake ruptures along the eastern boundary of the Sichuan-Yunnan faulted-block, southwestern China. Physics of the Earth and Planetary Interiors 168(1-2):16-36. https://doi.org/10.1016/j.pepi.2008.04.013

Wu WY, Xu C (2018) A new inventory of landslides triggered by the 2014 Ludian Mw 6.2 earthquake. Seismol Geol 40(5):1141-1148. (**in Chinese with English abstract**)

Xu C, Xu XW (2013) Response rate of seismic slope mass movements related to 2008 Wenchuan earthquake and its spatial distribution analysis. Chin J Rock Mech Eng 32(Supp 2):3889-3907. (**in Chinese with English abstract**)

Xu C, Xu XW, Shyu JBH (2015) Database and spatial distribution of landslides triggered by the

Lushan, China Mw 6.6 earthquake of April 20 2013. Geomorphology 248:77-92. https://doi.org/10.1016/j.geomorph.2015.07.002

Xu C, Wang SY, Xu XW, Zhang H, Tian YY, Ma SY, Fang LH, Lu RQ, Chen LC, Tan XB (2018) A panorama of landslides triggered by the August 8 2017 Jiuzhaigou, Sichuan Ms 7.0 earthquake. Seismol Geol 40(1):233-260. (**in Chinese with English abstract**)

Xu Q, Li WL (2010) Distribution of large-scale landslides induced by the Wenchuan earthquake. J Eng Geol 18(6):818-827. (**in Chinese with English abstract**)

Yu T, Li XJ (2015) Empirical estimation of VS30 in the Sichuan and Gansu province. China Earthq Eng J 37(2):525-533. (**in Chinese with English abstract**)

Yue X, Wu S, Yin Y, Gao J, Zheng J (2018) Risk identification of seismic landslides by joint Newmark and rockfall analyst models: A case study of roads affected by the Jiuzhaigou earthquake. Int J Disast Risk Sc 9(3):392-406. https://doi.org/10.1007/s13753-018-0182-9

Zhang B, Li XJ, Yu YX, Li N, Zhu J (2020) Comparison of strong ground motion records from Ludian, China, earthquake with ground-motion attenuation models. Chinese J Geophys-CH 63(8):2999-3014. (**in Chinese with English abstract**)

Zhang P, Deng Q, Zhang G, Ma J, Gan W, Min W, Mao F, Wang Q (2003) Active tectonic blocks and strong earthquake activities in the continent of China. Sci China Ser D 46(Supp):13-24. (**in Chinese with English abstract**)

Zhao SF, Shi BW, Xu J, Cui JW, Xu ZY (2019) Site predominant frequency of microtremor, equivalent shear wave velocity and classification of site soil in Kunming area. Prog Geophys 34(6):2533-2541. (**in Chinese with English abstract**)